Vibration Control of Flexible Beams Using Sensor Averaging and Actuator Averaging Methods

Ming-Chih Weng, Xiaodong Lu, and David L. Trumper, *Member, IEEE*

***Abstract*—Techniques are developed for suspension of flexible elements for noncontact handling in manufacturing processes. In support of this work, a magnetic suspension test bed are constructed, using eight actuators and eight sensors to control the flexible modes of a 3-m-long, 6.35-mm-diameter steel tube with varying boundary conditions. A novel approach has been developed for the control of such noncontact suspensions through sensor averaging and actuator averaging. The difficult stability and robustness problems imposed by the flexible dynamics of the work piece can be overcome by taking a properly weighted average of the outputs of a distributed array of motion sensors (sensor averaging), and/or by applying a properly weighted distributed array of actuating forces (actuator averaging) to the work piece. These approaches generate spatial filters on a broad range of undesired resonance modes without adversely affecting phase, and the resulting modal gains are independent of the specific boundary conditions and longitudinal dimensions of the work piece. The averaging arrangement can also eliminate possible noncollocation problems. These approaches are thus generally applicable to a wide range of structural control problems. In this paper, the averaging methods applied to beams are presented in detail. The experimental results with a beam suspension confirm the value of the averaging techniques, and suggest the wide future application of these ideas in industrial processes that require noncontact handling of work pieces.**

***Index Terms*—Magnetic levitation, noncontact processing, spatial filters, vibration control.**

I. Introduction

MANY industrial operations center on the processing of elongated axially moving elements; examples include steel rolling, plastic film production, paper production, coating, and painting. Noncontact handling by magnetic or electrostatic suspension can be advantageous for these manufacturing processes [1]–[3]. Our research in such systems was inspired by an idea developed by C. Smith for the production of painted metal handles for brooms and mops as shown in Fig. 1. The processing steps include forming and seam-welding, powder coating, induction heating, curing, water quenching, and cutting coated tubes into segments. In the sections between the powder coat and the water bath, the 47-m-long tube is supported by magnetic suspensions. There are ten suspension stations, with a spacing of 3–4 m between stations.

Manuscript received December 19, 2000; revised August 28, 2001. Manuscript received in final form October 14, 2001. Recommended by Associate Editor C. Knospe. This work was supported by the National Science Foundation under Grant DMI-9700973.

M.-C. Weng is with Seagate Technologies, Costa Mesa, CA 92626 USA.

X. Lu and D. L. Trumper are with the Department of Mechanical Engineering, Massachusetts Institute of Technology, Cambridge, MA 02139 USA.

Publisher Item Identifier S 1063-6536(02)01766-9.

The goal of our research is to stabilize such suspension systems with varying boundary conditions for different manufacturing processes. One of the greatest challenges with the suspension of flexible elements is to maintain stability of the high-frequency modes where the system has significant phase lag. Since the element is the product itself, we cannot change the damping of the structure; this makes the control design problem very challenging.

In support of the research, we have built a magnetic suspension testbed which uses eight actuators and eight sensors to control the flexible modes of a 3-m-long 6.35-mm-diameter 0.89-mm-wall-thickness steel tube. Fig. 2 is a photograph in our laboratory of the tubular beam suspended with free–free boundaries. The design of the sensors and actuators and preliminary experimental results are given in [4] and [5].

The vibration of such flexible structures is stabilized by two main approaches: 1) adding positive phase (damping) to the resonance modes at low frequencies by using a slow roll-up lead compensator and 2) reducing gains of the resonance modes to below 0 dB at high frequencies, where the system has significant phase lag due to sensor/actuator dynamics and computational and sampling time delay. The challenge of this control strategy is to reduce the gains at high frequencies without affecting the phase so much as to destabilize the system. Temperal notch filters have been widely used for this purpose, however, they are very sensitive to parametric uncertainties [6] and thus are not appropriate for systems with varying boundary conditions.

In this paper, we present theoretical and experimental results for *sensor averaging* and *actuator averaging*, which create nonmodel-based spatial filters that significantly attenuate selected modal gains. The simplest arrangement for sensor averaging places two sensors separated by a distance $2d_s$, and uses the averaged measurement as a single output for feedback. As shown later in detail, the resonance modes with wavelengths close to $4d_s$ will have low contribution to this averaged output. Actuator averaging is a dual to sensor averaging; the simplest arrangement places two actuators separated by a distance $2d_a$, and applies the same force to each actuator. This results in similar filtering effect for the resonance modes with wavelengths close to $4d_a$. It is shown that sensor/actuator averaging can attenuate modal gain over a broad range of undesired resonance modes without adversely affecting phase. One advantage of using the averaging method is that the resulting spatial filters depend only on the properties of the structural elements and the sensor/actuator arrangements, and is independent of boundary conditions and structure positions. Another advantage is that in the aver-

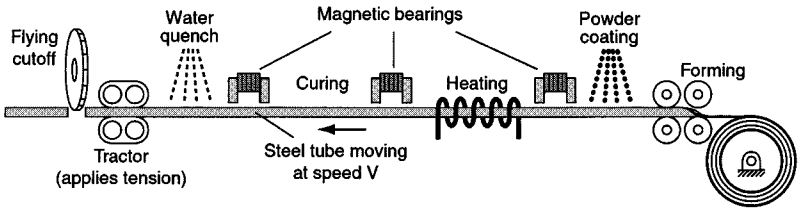

Fig. 1. Noncontact coating process for broom handles, as developed by Smith.

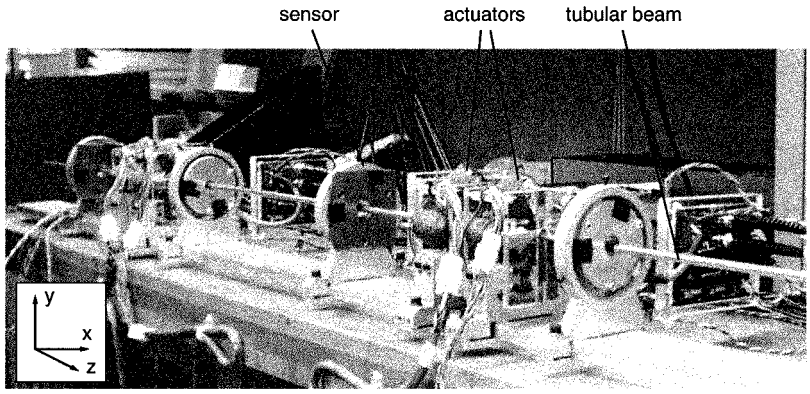

Fig. 2. Photograph of our scaled-model tube suspension.

aging arrangement, noncollocation problems can also be eliminated.

A related research area is the modal control method [7], which can be classified as a spatial filtering approach. The sensor/actuator averaging method attenuates the modal gain. On the other hand, the modal control method extracts modal coordinates, and applies modal forces to the vibration modes to be controlled. To extract modal coordinates, one can use modal filtering [8] or distributed sensing [9], [10]. Modal filtering uses multiple sensor outputs and calculated modal shapes to extract modal coordinates, but it requires a large number of sensors to avoid aliasing resonance modes with short wavelengths [11]. Distributed sensing uses continuous sensors of specific shapes to obtain modal coordinates of certain modes, it avoids aliasing modes with short wavelengths, but it can be very sensitive to location errors [12]. Most importantly, the modal control method is model-based and thus requires the knowledge of modal shapes. Hence, this approach does not suit our control problem with varying boundary conditions. The closest prior art is [13], which focuses on nonmodel-based distributed sensors.

This paper analyzes the filtering effect of the averaging methods on beams by modal analysis and demonstrate its utility by experiments with a tubular beam suspension. Further the averaging method is extended to multiple-sensor situations and to other distributed structures such as filaments, webs, and plates.

The remainder of this paper is organized as follows. Section II describes how the sensor averaging idea is developed. We formulate sensor averaging in Section III, its dual actuator averaging in Section IV, and their combination in Section V. Section VI is concerned with the controller design for our beam suspension. The experiment result is demonstrated in Section VII. Section VIII presents the extension of our averaging method, and we conclude the paper in Section IX.

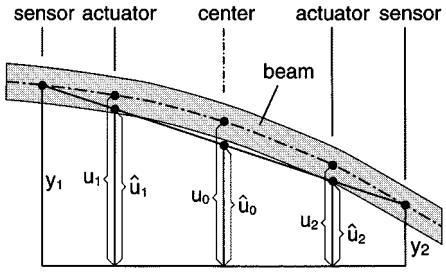

Fig. 3. Geometry of sensor interpolation: from measurement y_1 and y_2 calculate $\hat{u}_1$ and $\hat{u}_2$ by interpolation to estimate the real displacements u_1 and u_2 at the actuator locations. Sensor averaging utilizes the estimate $\hat{u}_0$.

II. Sensor Positioning

In this section, two sensor-positioning methods are described: interpolation and averaging. Sensor interpolation intends to eliminate sensor/actuator noncollocation problems, but was found to be overly sensitive to high-frequency resonance modes. Sensor averaging is designed to eliminate noncollocation problems and to simultaneously attenuate undesired resonance modes.

A. Sensor Interpolation

The sensor interpolation is developed in an attempt to eliminate possible sensor/actuator noncollocation problems. Here, two actuators between two sensors are placed in close proximity as shown in Fig. 3. Sensor outputs y_1 and y_2 are measured and $\hat{u}_1$ and $\hat{u}_2$ are calculated by interpolation, in an attempt to estimate the real displacements u_1 and u_2 at the actuators. In concept, the sensors and actuators can then be considered collocated and the controller design is less difficult. However, the gain of the estimated displacement to the real displacement $\hat{u}/u$ depends on the sensor/actuator location relative to each modal shape, with the exception when two actuators merge into one,

in which case interpolation becomes averaging, as is discussed next.

B. Sensor Averaging

Averaging is a special case of interpolation, where only one actuator is located at the midpoint between the two sensors. As shown in Fig. 3, the sensor outputs y_1 and y_2 is averaged to get $\hat{u}_0$ in order to predict the real displacement u_0 at the actuator. This approach has the property that the gain of the averaged displacement to the real displacement $\hat{u}_0/u_0$ is independent of the sensor/actuator location relative to the modal shape. Furthermore, it is found that a selected frequency range of resonance modes can be attenuated by adjusting the distance between sensors. With this overview in hand, in Sections III–IX we present the details of sensor averaging and its dual actuator averaging.

III. Sensor Averaging

In this section, the prospectives of the sensor averaging method is presented via modal analysis. As shown in Fig. 4 for the simplest case, we use the average of two sensors' measurements to represent a single point's displacement.

The beam without tensional force is represented by the Euler–Bernoulli beam equation [14]

$$EI\frac{\partial^4 u}{\partial z^4}+\rho A\frac{\partial^2 u}{\partial t^2}=f. \tag{1}$$

Here EI is the bending stiffness, u is the transverse deformation, z is the axial dimension, ρA is the mass per unit length, and f is an external transverse force density. The beam vibration is first represented by

$$u(z,t)=\sum_{n=1}^{\infty}\xi_n(t)\phi_n(z) \tag{2}$$

where $\xi_n(t)$ is the nth modal coordinate and $\phi_n(z)$ is the nth modal shape

$$\phi_n(z)=(C_{n1}\cos k_n z+C_{n2}\sin k_n z +C_{n3}\cosh k_n z+C_{n4}\sinh k_n z). \tag{3}$$

The associated beam dispersion equation is

$$k_n=\sqrt[4]{\frac{\rho A\omega_n^2}{EI}} \tag{4}$$

where the wavenumber k_n and the modal frequency ω_n are related, and can be determined from boundary conditions. The main control problem is with the high-frequency modes of slender structures. Thus, the evanescent waveforms near the boundaries are less important, and we assume the beam vibration is dominated by the sinusoidal terms. Thus, the beam vibration is approximated by

$$u(z,t)=\sum_{n=1}^{\infty}\xi_n(t)(C_{n1}\cos k_n z+C_{n2}\sin k_n z). \tag{5}$$

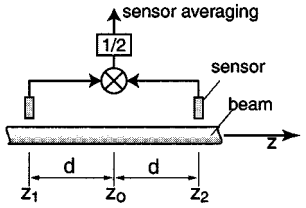

Fig. 4. Sensor positioning arrangement in two-sensor averaging.

For two sensors set apart by a distance of $2d$ as shown in Fig. 4, the averaged output $\hat{u}(z_0,t)$ is given by

$$\begin{aligned}\hat{u}(z_0,t)=&\frac{1}{2}(u(z_1,t)+u(z_2,t))\\ =&\frac{1}{2}\sum_{n=1}^{\infty}\xi_n(t)[\phi_n(z_1)+\phi_n(z_2)].\end{aligned} \tag{6}$$

With sensors located at $z_1=(z_0-d)$ and $z_2=(z_0+d)$, the averaged output of nth mode is

$$\begin{aligned}\frac{1}{2}[\phi_n(z_1)+\phi_n(z_2)]=&\frac{1}{2}[C_{n1}(\cos k_n z_1+\cos k_n z_2)\\ &+C_{n2}(\sin k_n z_1+\sin k_n z_2)]\\ =&(C_{n1}\cos k_n z_0+C_{n2}\sin k_n z_0)\cos k_n d\\ =&\phi_n(z_0)\cos k_n d.\end{aligned} \tag{7}$$

After placing this result into (6), the averaged output is

$$\hat{u}(z_0,t)=\sum_{n=1}^{\infty}\xi_n(t)\phi_n(z_0)\cos k_n d. \tag{8}$$

This is one key result. By averaging, a modal band-stop filter is created, where each mode has a gain of $\cos k_n d$. Replacing wavenumber k_n by frequency ω_n from (4), the cosine effect $\cos k_n d$ becomes

$$\cos k_n d=\cos\left(\sqrt[4]{\frac{\rho A\omega_n^2}{EI}}d\right). \tag{9}$$

Using the parameters from our tubular beam experiment, with $\rho A/EI=0.01$, by choosing $d=0.15$ m, the result is as illustrated in Fig. 5. If the modal gain is plotted as a function of wavenumber k_n, it is simply a cosine function. The notch zero is located at $k_n d=\pi/2$. Since wavelength $\lambda_n=2\pi/k_n$, this notch corresponds to a mode with wavelength of $4d$. When the modal gain is plotted as a function of resonance frequency ω_n, the resulting plot shows that resonance modes are attenuated near the notch zero at $\omega_n\approx 1000$ rad/s (wavelength $=$ 0.60 m). The phase stays unchanged before the notch, and flips by 180° after the notch when $\cos k_n d<0$. The result shows a very promising potential: *if we adjust the sensor spacing $2d$, we can attenuate undesired resonance modes without adversely affecting the phase below the notch*. Furthermore, at frequencies below the cosine notch, all the resonance modes are in phase, which means there will be no sensor/actuator noncollocation problems for these modes.

To demonstrate this cosine effect on beam dynamics, the transfer function from an actuating force

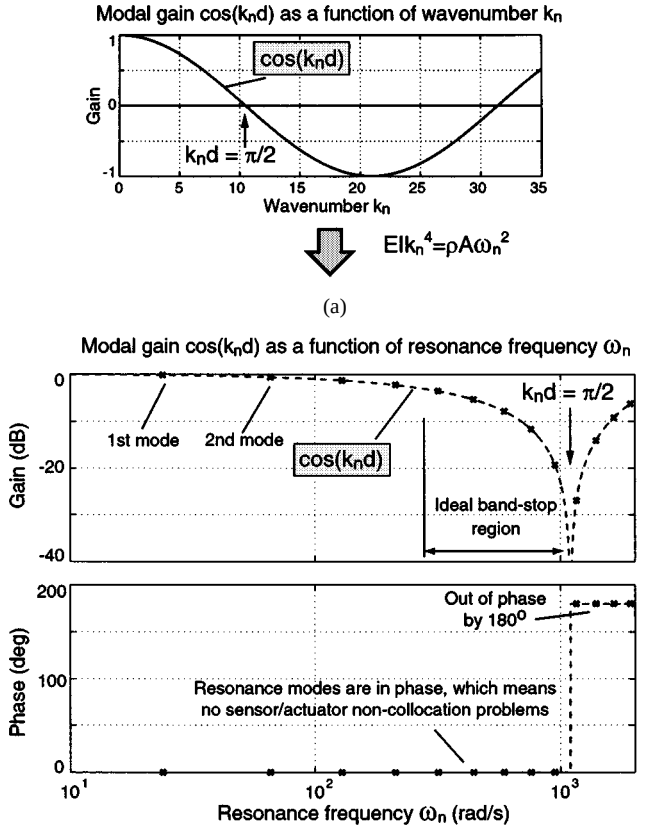

Fig. 5. Two-sensor averaging for beams: modal gain $\cos k_n d$ plotted as (a) function of k_n and (b) function of ω_n.

$f(t)$ concentrated at z_0 to the sensor averaging ouput $\hat{u}(t)$ $(= (1/2)(u(z_1,t) + u(z_2,t)))$ can be written by modal analysis as

$$\frac{\hat{u}(s)}{f(s)} = \sum_{n=1}^{\infty} \left(\frac{\phi_n^2(z_0)}{M_n\,(s^2 + 2\zeta_n\omega_n s + \omega_n^2)} \cdot \cos k_n d \right). \quad (10)$$

The modal gain $\cos k_n d$ attenuates the resonance modes over a broad range of frequencies without adversely affecting the phase. The bode plot of this transfer function is shown in Fig. 6 for a built-in beam of length $L = 3$ m and actuator location $z_0 = 1$ m.

If the cosine notch is put at the frequency region where there are modes which destabilize the control loop, (gain $>$ 0 dB, phase $< -180^\circ$), this notch attenuates the resonance peaks at that region without affecting the phase, and thereby increases the system gain margin, improving the stability-robustness.

The result (10) shows that averaging yields a nonmodel-based modal-band-stop filter with the following properties:

1) It is independent of sensor pair location z_0.
2) It is independent of boundary conditions. When boundary conditions change, the natural frequencies associated with k_n change. That is, in Fig. 5, the curve remains the same, although the modes (shown as crosses) move along the curve.
3) The undesirable 180° phase flip above the notch can be easily eliminated by actuator averaging, which will be discussed in Section IV.

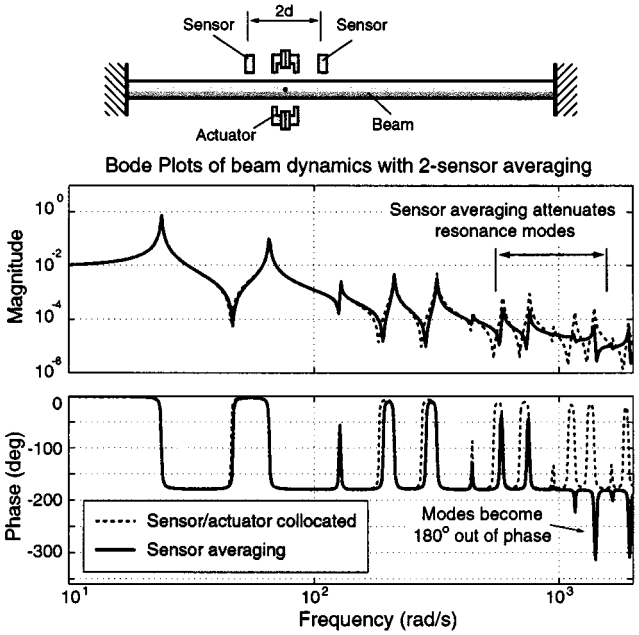

Fig. 6. Theoretical transfer function of beam model for two-sensor averaging. Solid line shows results with two-sensor averaging $(d = 15$ cm). Note that a broad range of resonance modes is attenuated. Dashed line shows results with collocated sensor and actuator $(d = 0)$cm for comparison.

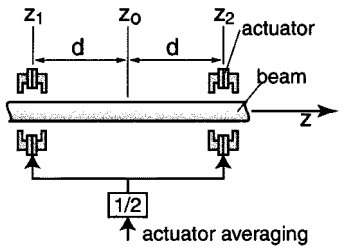

Fig. 7. Actuator positioning arrangement in two-actuator averaging.

IV. Actuator Averaging

Actuator averaging is the dual to sensor averaging. As shown in Fig. 7, the simplest form of actuator averaging uses two actuators with the same force applied to each actuator. The resulting filtering effect is quite similar to sensor averaging. Sensor averaging is easier to understand since it simply averages the vibration waveforms. Actuator averaging places actuators in a similar way such that certain resonance modes will not be excited. This idea can be understood via the concepts of modal force as described below.

The duality of sensor averaging and actuator averaging is shown by using the beam example. We place two actuators set apart by $2d$, and apply the same control forces $(1/2)\hat{f}$ to each actuator. As before we assume the modal shapes are sinusoidal. With actuators located at $z_1 = (z_0 - d)$ and $z_2 = (z_0 + d)$, the averaged nth modal force N_n is given by

$$\begin{aligned} N_n &= \int_0^L f(z)\phi_n(z)dz \\ &= \int_0^L \frac{1}{2}\hat{f}(t)(\delta(z - z_1) + \delta(z - z_2)) \cdot \phi_n(z)dz \\ &= \frac{1}{2}\hat{f}(t)(\phi_n(z_1) + \phi_n(z_2)) \\ &= \hat{f}(t)\phi_n(z_0)\cos k_n d. \end{aligned} \quad (11)$$

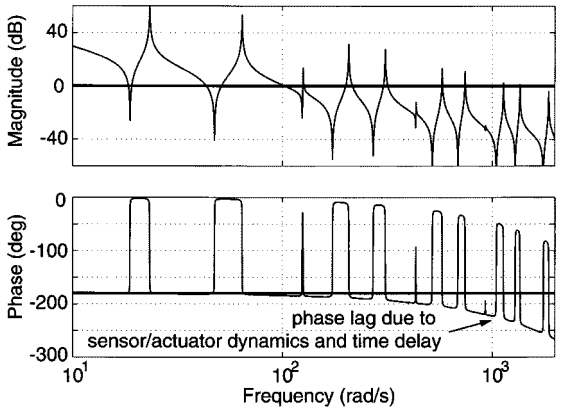

Fig. 8. Bode plots of open-loop dynamics, from collocated force input command to sensor output voltage, including dynamics of beam, sensor, actuator and time delay, assuming damping ratio $\zeta = 0.001$.

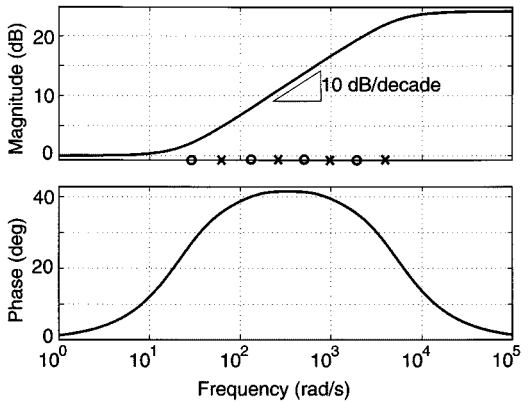

Fig. 9. Bode plots of a slow roll-up lead compensator. The breakpoints associated with each pole and zero are labeled on the frequency axis.

Here $\hat{f}(t)\phi_n(z_0)$ is the modal force associated with one actuator with force $\hat{f}(t)$ concentrated at $z = z_0$. The averaged modal force has a gain of $\cos k_n d$ just like the sensor averaging method, and thus we can develop plots similar to those of Fig. 6 for actuator averaging.

V. Combination of Sensor Averaging and Actuator Averaging

Sensor averaging and actuator averaging are most advantageously used in combination. In this case, the filter gain of each mode is the multiplication of both averaging effects. For beams, using two sensors set apart by $2d_s$ and two actuators set apart by $2d_a$, the frequency response from average actuator input to average sensor output becomes

$$\frac{\hat{u}(s)}{\hat{f}(s)} = \sum_{n=1}^{\infty} \frac{\phi_n^2(z_0)}{M_n\left(s^2 + 2\zeta_n\omega_n s + \omega_n^2\right)} \cos k_n d_s \cos k_n d_a. \tag{12}$$

In other words, the filter gain of each mode becomes $\cos k_n d_s \cdot \cos k_n d_a$. The distances d_s and d_a can be arranged to meet the system's requirement. For instance, if $d_s = d_a$, coincident notches are created, and the 180° phase flip is eliminateed. Alternately, if the spacings are unequal, stagger-tuned notches are created and thus a broaden region of significant modal attenuation is achieved.

VI. Controller Design

The challenges of controlling levitated flexible structures result from the following.

1) A levitated structure has a low damping ratio ζ, and thus the modes have high peaks in the transfer function. In our experiment, we measure $\zeta \approx 0.001$ for free–free boundaries. This means that a very broad range of modes have an impact on loop stability.
2) Because of the sensor dynamics, actuator dynamics and computational and sampling time delay, the control systems usually have significant phase lag within the desired bandwidth.

Fig. 8 shows the modeled plant dynamics of our experiment, including dynamics of the beam, actuator, sensor, and time delay (computational time and half sampling time due to ZOH). This plant assumes a collocated sensor and actuator at $z_0 = 1$ m, for the experimental 3-m-long beam.

The first task of the controller is to add positive phase to the modes that we want to control. A *slow roll-up lead compensator* is designed, and this is a single-input–single-output (SISO) multiple-lead compensator. This compensator has the following structure:

$$H(s) = K_p \frac{(s+m)(s+4m)(s+16m)\ldots}{(s+2m)(s+8m)(s+32m)\ldots}. \tag{13}$$

The controller frequency response is shown in Fig. 9 for four sets of pole-zero pairs and m is set as 30.

This controller will provide a phase margin of about 30 degrees for the frequencies of interest. It has gain rolling up at an average slope of 10 dB/decade to avoid overamplifying resonance peaks at high frequencies. Depending upon the design requirements and structural damping ratio, the spacing ratio of the zero-pole locations can be changed to have more phase margin or a slower roll-up rate, and the phase compensated region can be changed by adjusting m. To increase the low-frequency stiffness and to get zero steady-state error, an integration term $(1 + T_s s)/(T_s s)$ is also added into the controller.

For the free–free-boundary beam suspended by multiple sensor/actuator sets, a diagonal multiple-input–multiple-output (MIMO) controller is designed by the sequential loop closing method [15] to stabilize the beam. This controller architecture is shown in Fig. 10. Sets of two actuators and two sensors are used to implement actuator and sensor averaging. There are four such sets acting on the beam.

The input and output of the sensor/actuator sets are associated with four individual SISO controllers, which are tuned sequentially to stabilize each loop. The effects of sensor/actuator averaging can be seen in the broad range of modal attenuation in the vicinity of 1000 rad/s as compared to the collocated case of Fig. 8. Because of this attenuation, the controller gain can be made relatively large in order to stiffen the suspension and thus better constrain the tube motion from external disturbance.

VII. Experimental Result

This section shows experimental results from one scaled tubular beam magnetic suspension for both clamped–clamped and free–free boundary conditions.

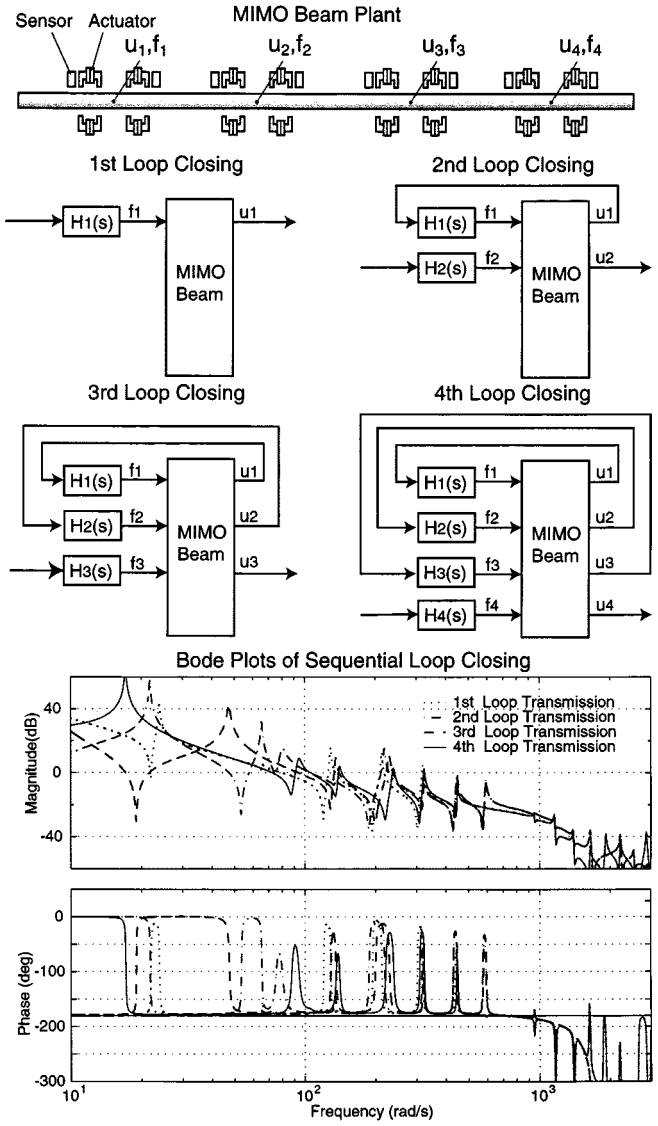

Fig. 10. Sequential loop closing for the MIMO beam controller design.

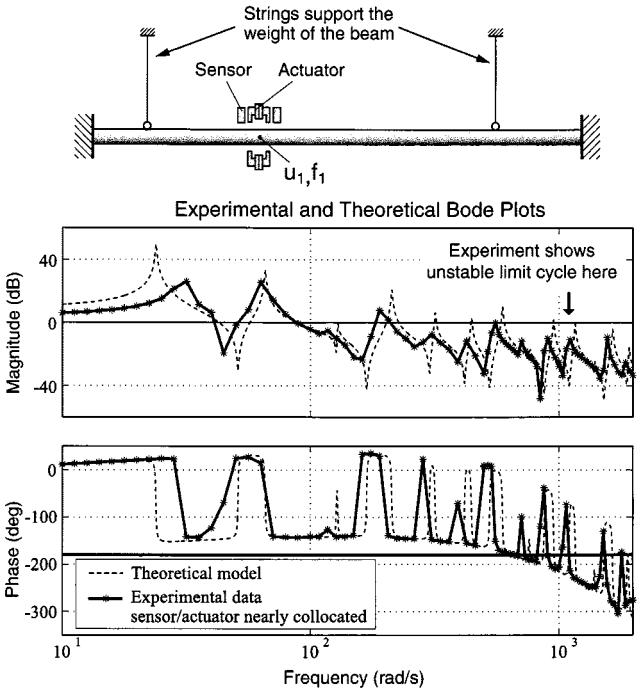

Fig. 11. Experimental setup and Bode plots of loop transfer function using collocated sensor/actuator. Dashed line shows theoretical Bode plots for comparison.

A. Experimental Setup

In an experiment (Fig. 2), eight sensors and eight actuators are used to suspend the steel tube. Both sensors and actuators have 2.7 mm bores. The tube is steel, with a mass per unit length $\rho A = 0.1190$ kg/m, Young's modulus $E = 200$ GPa, outside diameter $\phi = 6.35$ mm, wall thickness $w = 0.89$ mm, and length $L = 3$ m. The experiment controller is implemented on a digital signal processing (DSP) board with a sampling time of 250 μs. Total computational time is about 220 μs, thus the controller is almost completely utilized.

B. Control With Nearly Collocated Sensor/Actuator

The beam is clamped at both ends, support the beam weight by two elastic bands, and place one actuator at the center between two sensors to control the beam at the point $z = 1.12$ m. We place the sensors and actuator in close proximity, hence we can consider the sensors and the actuator as essentially collocated (or more precisely, sensor averaging with notch zero at a frequency higher than 5000 rad/s). With the plant input as force in Newtons and the sensor output in meters, the controller takes the form

$$H(s) = 4\frac{(s+30)(s+120)(s+400)^2}{(s+60)(s+240)(s+800)^2}. \tag{14}$$

With this controller, we are almost able to stabilize the system, except that there is a limit cycle vibration at 1100 rad/s. Fig. 11 shows the experimental setup and the measured loop transfer function $H(s)G(s)$ compared with our theoretical model.

The loop has 30° phase margin for all vibration modes below 500 rad/s. The alternating pole-zero pattern shows that there is no noncollocation problem. The discrepency in the first mode between the thoretical model and the experiment result comes from the string that is attached with a soft spring to partly support the weight of the beam, and the unmodeled spring helps to increase the natural frequency of the low-frequency modes.

C. Control With Two-Sensor Averaging

To avoid the limit cycle in the collocated sensor/actuator experiment, we pull the sensors apart to implement sensor averaging. Specifically, the sensors are placed ± 0.15 m from the actuator at $z = 1.12$ m. We use the same controller as in Section VII-B. Fig. 12 shows the experimental setup and the measured loop transfer function compared to the collocated sensor/actuator experiment. The sensor averaging shows an improvement of gain margin within frequency range from 700 rad/s to 1500 rad/s while the phase is below $-180°$. Thus, we are able to stabilize the system and avoid the limit cycle. Notice

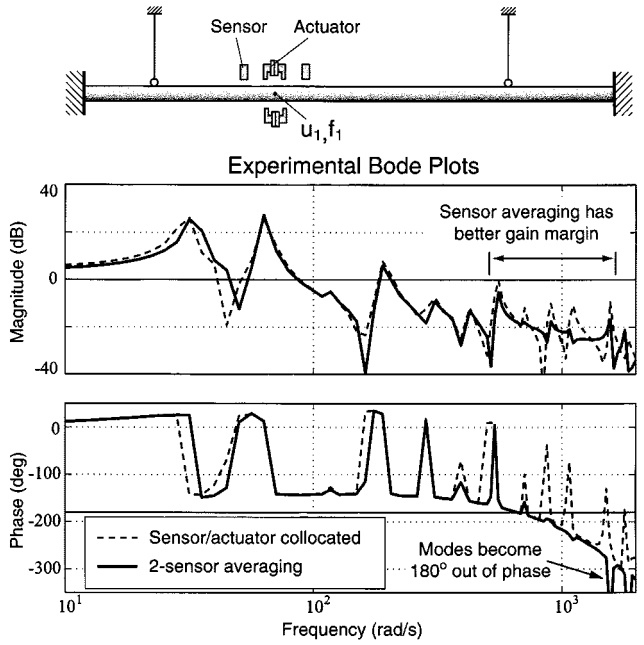

Fig. 12. Experimental setup and Bode plots of loop transfer function using two-sensor averaging. Dashed line shows the previous result of collocated sensor/actuator experiment for comparison.

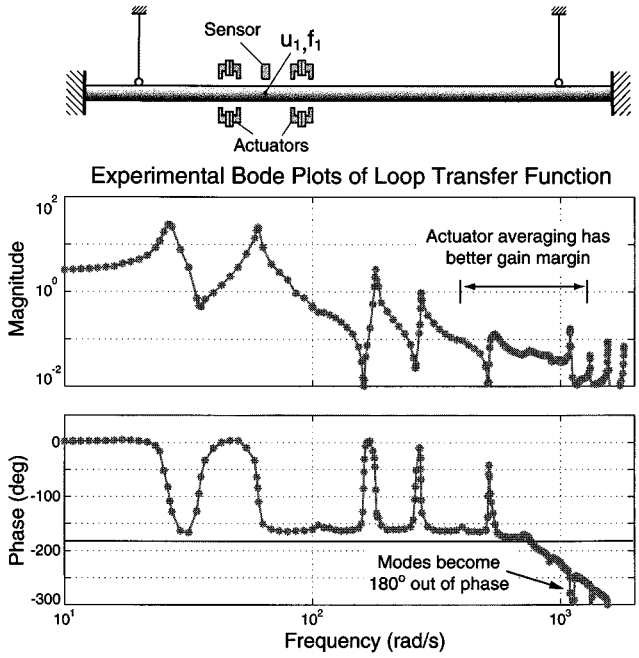

Fig. 13. Experimental setup and Bode plots of loop transfer function by using two-actuator averaging.

the modal gain becomes 180° out of phase after the cosine notch zero.

D. Control With Two-Actuator Averaging

To verify the effectiveness of actuator averaging, we use one sensor and two actuators to implement this experiment. Specifically, the sensor is placed at $z = 1.12$ m, and the actuators are placed ± 0.17 m from the sensor. Fig. 13 shows the experimental setup and the measured loop transfer function. Notice the duality between this setup and sensor averaging.

E. Control of Free Beam With Sensor Averaging and Actuator Averaging

While the tubular beam is being suspended with free–free boundaries, the damping ratio of the beam is measured to be below 0.001. We add actuator averaging along with sensor averaging to create a broader notch, which creates two adjacent cosine notches. The suspended tube shows robust stability when the boundary conditions varies, including simply supported, clamped, and free boundaries. The experimental setup and measured Bode plots of the loop transmission at the second point with all loops closed is shown in Fig. 14. Here two notches resulting from sensor averaging and actuator averaging can be found at 900 rad/s and 1200 rad/s, respectively. The nonminimum phase zero observed around 600 rad/s is not predicted by our analyzes, but this zero does not destabilize the closed-loop system. This nonminimum phase zero may arise from two possiblities. We feedback linearize the actuator force–current–displacement relation to control the actuator force output, but in implementing this algorithm, the averaged sensor output must be used because the actual displacement of the beam at the actuator location is not measured. Another possible cause is the inaccuracies in the location of the sensors

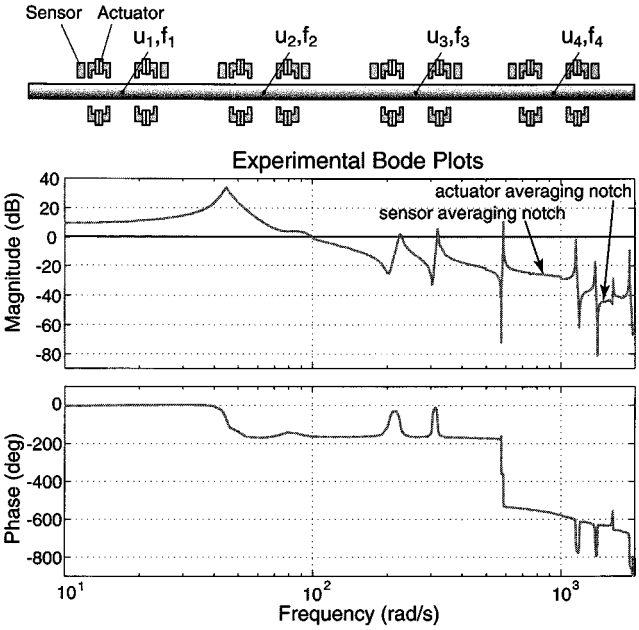

Fig. 14. Experimental setup and Bode plots of loop transfer function at the second point with all loops closed, and using both sensor averaging and actuator averaging. The flattened regions are the result of this averaging.

and actuators in each set. As the nonminimum phase zero causes no stability problems (it is just slightly in the right half plane) we have not investigated this issue further.

VIII. Extension of Sensor Averaging/Actuator Averaging

Given the advantage of sensor averaging/acutor averaging methods in the beam vibration control, we extend this method to multiple sensor/actuator arrangment. As actuator averaging is a dual to sensor averaging, here we discuss only the extension of

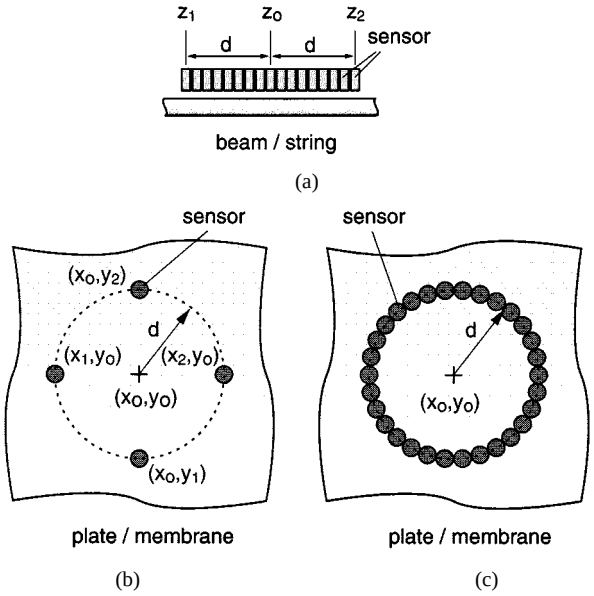

Fig. 15. Multisensor averaging arrangement for (a) beams and (b) and (c) plates/membranes.

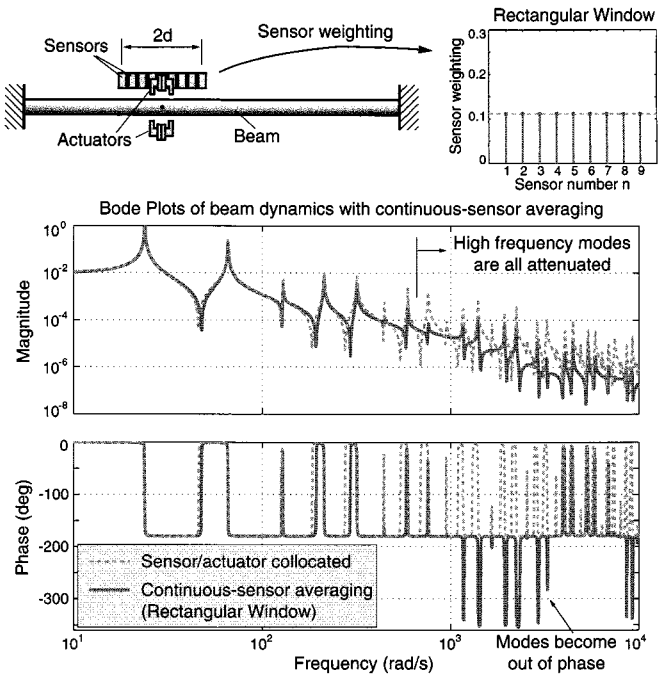

Fig. 16. Theoretical beam model for nine-sensor averaging with a rectangular window. The solid line shows a beam model with nine-sensor averaging with a rectangular window ($d = 30$ cm); the resonance modes at high frequencies are all attenuated. Dashed line shows a beam model with collocated sensor and actuator ($d = 0$)cm for comparison.

sensor averaging and all conclusions from sensor averaging are also applicable to actuator averaging. In [18], all conclusion for beams are further generalized to strings, membranes, and plates.

The logical extension of the sensor averaging at two points is to use more sensors. The limit is continuous position sensing as shown in Fig. 15(a). From the previous derivation, we realize that sensor averaging is a spatial filter, and is a dual to a temporal filter. Therefore we can adopt the filter theory widely used for signal processing [16] and apply it to sensor averaging. In the following, we demonstrate the characteristics of continuous-sensor averaging using rectangular, triangular, and Blackman windows.

Rectangular Window: By using a rectangular window, we have the same weightings for all sensors. We assume that we have an infinite number of sensors placed within the length $2d$, the averaged output is chosen to be the integration of all sensor output

$$\hat{u}(z_0,t) = \frac{1}{2d}\int_{z_1}^{z_2} u(z,t)dz = \sum_{n=1}^{\infty}\left(\xi_n(t)\phi_n(z_0)\cdot\frac{\sin k_n d}{k_n d}\right). \quad (15)$$

The modal gain is a sinc function $(\sin k_n d)/(k_n d)$. This has a notch zero at $k_n d = \pi$, and has a 180° phase flip after the notch zero. Notice that the high-frequency modes will be attenuated, which is the main advantage of using continuous sensing.

Use our experimental setup as a numerical example, and assume that we have nine sensors over 0.60-m span, the sensor weighting for each sensor is 0.1111. The resulting beam dynamics are shown in Fig. 16. Notice that the resonance modes become out of phase after the notch zero.

Triangular Window (Bartlett Window): A triangular window is known to have a slightly wider mainlobe, and slightly lower sidelobes than a rectangular window. Using the experimental setup as a numerical example, we assume nine sensors placed along a 1.20-m span. The sensor weightings are: 0.04, 0.08, 0.12, 0.16, 0.20, 0.16, 0.12, 0.08, and 0.04, respectively. The resulting beam dynamics are shown in Fig. 17. Notice that the phase remains unchanged above the notch, which is the main advantage of using a triangular window.

Blackman Window: The Blackman window is known to have sidelobes lower than −60 dB. The tradeoff is that it has a wide mainlobe, hence we need a longer space to place sensors. Using our experimental setup as a numerical example, we assume nine sensors placed along 1.20 m. The sensor weightings are: 0.0096, 0.0478, 0.1214, 0.2022, 0.2381, 0.2022, 0.1214, 0.0478, and 0.0096, respectively. The resulting beam dynamics are shown in Fig. 18. Note that the high-frequency modes become almost unobservable. Another significant advantage of using a Blackman window is that the gain falls at a slope of −2 at high frequencies as compared with the original dereverberated transfer function (backbone) of the original dynamics that falls at a slope of −1.5.

IX. Conclusion

This paper presents the novel concepts of sensor averaging and actuator averaging for vibration control of flexible elements. This method makes use of the relations between resonance frequencies and wavelengths as they depend on structural properties, and which can be calculated analytically. Therefore, we can place sensors and actuators based on the wavelengths of undesired modes, and attenuate these resonance modes to improve the loop gain margin. This averaging method is mathematically proven and experimentally verified. The method creates

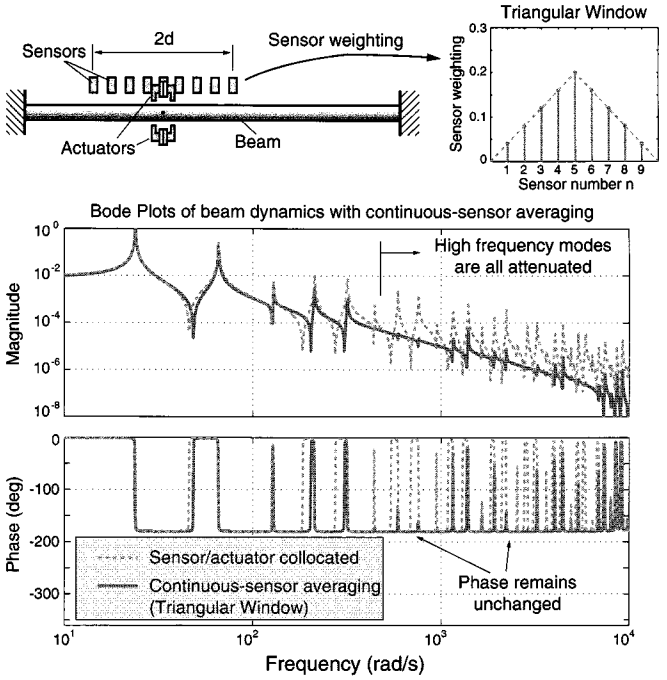

Fig. 17. Theoretical beam model: nine-sensor averaging with a triangular window. The solid line shows a beam model with nine-sensor averaging with a triangular window ($d = 60$ cm). The phase remains unchanged above the notch. Dashed line shows a beam model with collocated sensor and actuator ($d = 0$)cm for comparison.

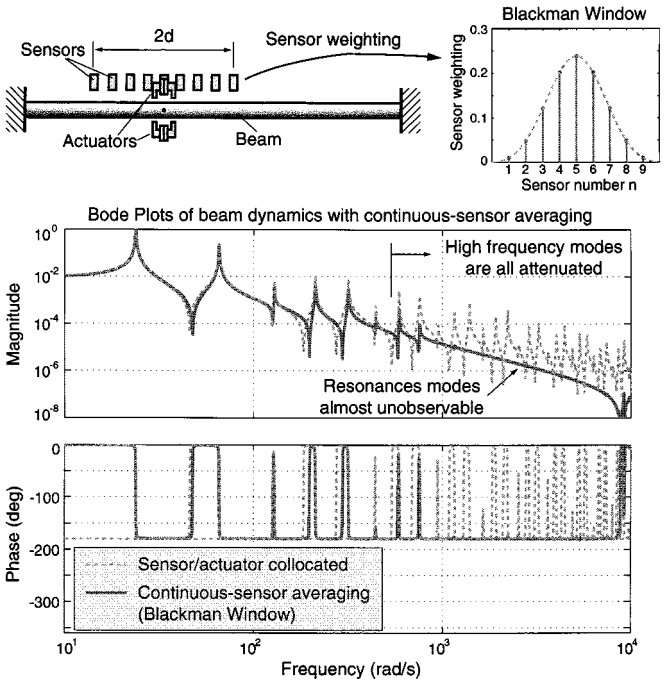

Fig. 18. Theoretical beam model: nine-sensor averaging with a Blackman window. The solid line shows a beam model with nine-sensor averaging with a Blackman window ($d = 60$ cm). The resonance modes at high frequencies are almost unobservable. Dashed line shows a beam model with collocated sensor and actuator ($d = 0$)cm for comparison.

spatial filters to attenuate vibration modes without adversely affecting the loop phase. In the experiment of beam suspension, we simply design the frequency range we want to attenuate the modal gain, calculate the corresponding wavenumber k_n, and then choose the averaging distance d such that $k_n d \approx (\pi/2)$.

The resulting modal gain is independent of sensor/actuator pair location, namely z_0 for beams/strings and (x_0, y_0) for plates/membranes. It is also independent of boundary conditions; thus the method is quite robust. Although in this paper we use frequency domain control for our application, this averaging method can be used in state-space control as well. Furthermore, in open-loop control, actuator averaging can be used to avoid exciting certain resonance modes.

The main limitation of our analysis is that we assume sinusoidal modal shapes, and thus neglect the evanescent waveforms. This assumption is acceptable when the sensors and actuators are one wavelength away from the boundaries of a slender suspended member for high-frequency mode. The approximation is especially applicable at high frequencies where the wavelengths are short. The resulting analytical simplification allows the development of averaging concepts.

ACKNOWLEDGMENT

The authors wish to thank Professor J. H. Lang and Professor S. Nayfeh at MIT for their helpful comments.

REFERENCES

[1] Y. Oshinoya and T. Shimogo, "Electro-magnetic levitation control of an elastic plate," in *Proc. Maglev '89*, 1989, pp. 435–440.
[2] H. Hayasiya, H. Ohsaki, and E. Masada, "Magnetic levitation control of elastic steel plate for steel making process," in Proc. ICEE '95, 1995.
[3] J. Jin, T. C. Yih, T. Higuchi, and J. U. Jeon, "Direct electrostatic levitation and propulsion of silicon wafer," *IEEE Trans. Ind. Applicat.*, vol. 34, pp. 975–984, 1998.
[4] D. L. Trumper, M. C. Weng, and R. J. Ritter, "Magnetic suspension and vibration control of beams for noncontact processing," in *Proc. IEEE CCA-CACSD '99*, 1999, pp. 551–557.
[5] M. C. Weng and D. L. Trumper, "A design method for magnetic suspension and vibration control of levitated beams for noncontact processing," in Proc. NASA ISMST-5 '99, 1999.
[6] B. Wie, "Active vibration control synthesis for the control of flexible structures mast flight system," *AIAA J. Guidance, Contr., Dyn.*, vol. 11, no. 3, pp. 271–277, 1988.
[7] M. J. Balas, "Active control of flexible systems," *J. Optimization Theory Applicat.*, vol. 25, no. 3, pp. 415–436, 1978.
[8] L. Meirovitch and H. Baruh, "The implementation of modal filters for control of structures," *AIAA J. Guidance, Contr., Dyn.*, vol. 8, no. 6, pp. 707–716, 1985.
[9] T. Bailey and J. E. Hubbard, "Distributed piezoelectric-polymer active vibration control of a cantilever beam," *AIAA J. Guidance, Contr., Dyn.*, vol. 8, pp. 605–611, 1985.
[10] C.-K. Lee and F. C. Moon, "Modal sensors/actuators," *ASME J. Appl. Mech.*, vol. 57, pp. 434–441, 1990.
[11] C. R. Fuller, S. J. Elliott, and P. A. Nelson, *Active Control of Vibration*. New York: Academic, 1997, ch. 5.
[12] R. L. Clark and S. E. Burke, "Practical limitations in achieving shaped modal sensors with induced strain materials," *ASME J. Vibration Acoust.*, vol. 118, no. 4, pp. 668–675, 1996.
[13] S. A. Collins, D. W. Miller, and A. H. von Flotow, "Distributed sensors as spatial filters in active structural control," *J. Sound Vibration*, vol. 173, no. 4, pp. 471–501, 1994.
[14] L. Meirovitch, *Elements of Vibration Analysis*. New York: McGraw-Hill, 1975, ch. 5.
[15] J. M. Macijowski, *Multivariable Feedback Design*. Reading, MA: Addison-Wesley, 1989, ch. 4.
[16] A. V. Oppenheim and R. W. Schafer, *Discrete-Time Signal Processing*. Englewood Cliffs, NJ: Prentice-Hall, 1989, ch. 7.
[17] J. A. Wickert and C. D. Mote Jr, "Classical vibration analysis of axially moving continua," *ASME J. Appl. Mech.*, vol. 57, pp. 738–744, Sept. 1990.
[18] M.-C. Weng, "Magnetic suspension and vibration control of flexible structures for non-contact processing," Ph.D. dissertation, Massachusetts Inst. Technol., Cambridge, MA, 2000.

Ming-Chih Weng received the B.S. degree in mechanical engineering from National Taiwan University, Taipei, Taiwan, in 1991 and the M.S. and Ph.D. degrees in mechanical engineering from Massachusetts Institute of Technology, Cambridge, in 1995 and 2000, respectively.

He is currently with Seagate Technologies, LLC, Costa Mesa, CA. His research interests include mechatronics, structural vibrations, control system design, and mechanical design.

Xiaodong Lu received the B.S. and M.S. degrees in automotive engineering from Tsinghua University, China, in 1997 and 1999, respectively. He is currently pursuing the doctoral degree in mechanical engineering at Massachusetts Institute of Technology, Cambridge.

His research topics include magnetic suspension and vibration control of flexible structures and fast tool servos.

David L. Trumper (S'80–M'90) received the B.S., M.S., and Ph.D. degrees in electrical engineering and computer science from Massachusetts Institute of Technology (MIT), Cambridge in 1980, 1984, and 1990, respectively.

Following the Bachelor's degree, he worked two years for Hewlett-Packard. After finishing the Master's degree, he worked for two years for the Waters Chromatography Division of Millipore. Upon completing the Ph.D. degree, he was an Assistant Professor in the Electrical Engineering Department at the University of North Carolina at Charlotte, Charlotte, for three years, working within the precision engineering group. In 1993, he joined the Department of Mechanical Engineering, MIT, and is currently an Associate Professor. His research interests are in the area of the control of electromechanical systems with a specialization in precision motion control, high-performance manufacturing equipment, and magnetic suspensions and bearings.

Dr. Trumper is a Member of the ASME, SME, ASPE, and JSPE and is a corresponding member of CIRP. He is an Associate Editor of *Precision Engineering*.